On the inverse kinetic-energy cascade in premixed isotropic turbulent flames

Xiang Qian, Hao Lu*, Chun Zou†, Hong Yao

State Key Laboratory of Coal Combustion,

School of Energy and Power Engineering,

Huazhong University of Science and Technology, Wuhan 430074, China

July 6, 2021

Abstract

The understanding of energy transfer in fluids is important for the accurate modeling of turbulent reacting flows. In this study, we investigate interscale kinetic-energy transfer and subgrid-scale (SGS) backscatter using data from direct numerical simulations (DNSs) of premixed isotropic turbulent flames. Results reveal that in the examined premixed flames, the pressure-transfer term appearing in the transport equation of turbulent kinetic energy dominates the nonlinear advection and the dissipation at large scales, and noticeably contributes to the inverse kinetic-energy cascade. Filtered DNS data show that SGS backscatter is correlated with the appearance of positive pressure-dilatation work, i.e. thermal expansion. *A priori* test results of three SGS stress models reveal that the Smagorinsky stress model is unable to capture SGS backscatter, but that two nonlinear structural stress models are able to predict SGS backscatter.

Keywords Turbulent premixed flame; Direct numerical simulation; Subgrid scale

1 Introduction

The energy-cascade hypothesis states that turbulent kinetic energy is transferred from large to smaller and smaller scales until it is dissipated by viscosity. However, the inverse transfer of kinetic energy from small to large scales (also known as 'inverse energy cascade' or 'backscatter') may noticeably occur in turbulent premixed [1, 2] and diffusion flames [3], contrary to the net transfer of kinetic energy from large to small scales in non-reacting turbulence [4]. It is better to consider the directions (forward and inverse) of kinetic-energy transfer in subgrid-scale (SGS) modeling [5, 6], particularly for large-eddy simulation (LES) of turbulent combustion.

Analysis of inverse kinetic-energy cascade can be carried out in Fourier space or in physical space, although there may not be a simple relationship between them [5, 3]. Spectral

*E-mail: haolu@hust.edu.cn

†E-mail: zouchun@hust.edu.cn

analysis in Fourier space helps to unravel the scaling characteristics of physical fields. Early studies including experiments and direct numerical simulations (DNSs) [7, 8] focused mainly on the spectral features of velocities and scalars under the influence of combustion. For instance, the experimental study by Furukawa et al. [7] is one of the earliest attempts to measure the Kolmogorov scale within the local reaction zone of a turbulent premixed flame. Kolla et al. [8] have presented evidence that high-wavenumber modes of the spectra of kinetic energy and reactive scalars in turbulent premixed flames do not adhere to classical incompressible scaling laws. Very few attempts have been made to explore the energy transfer in Fourier space. Using data from a DNS of a statistically planar turbulent premixed flame, Tower et al. [1] have shown that nonlinear advection is the key factor leading to inverse kinetic-energy cascade in the flame brush close to products, but research has yet to uncover the effects that pressure has on kinetic energy.

Inverse kinetic-energy cascade appears physically in anisotropic turbulent flows, including rotating turbulence [9], boundary layers [10], mixing layers [11], and reacting flows [3, 2]. O'Brien et al.'s [3, 2] DNS data of a turbulent diffusion flame [3] and a turbulent premixed flame [2] show that SGS backscatter occurs primarily in regions undergoing volumetric expansion. However, their studies cannot completely isolate the anisotropies caused by turbulent mixing of fuel and oxidizer [3] or productions and reactants [2].

The research community has lacked a satisfactory grasp of how heat release in combustion reactions can affect the interscale transfer of kinetic-energy. To bridge this gap, in the current study, we adopt the isotropic-turbulence configuration with periodic boundary conditions in three directions. Isotropic turbulence is an idealized turbulent flow free from the influences of flow anisotropy. For the most part, classical statistics in the field of turbulence mostly rest on the isotropic assumption [12], and many theories are widely used in research on turbulent combustion [13] (such as Kolmogorov scalings). In this study, we address the problem of a premixed flame in isotropic turbulence with non-unity Lewis numbers. We focus on quantifying the relationship between pressure and backscatter. Moreover, in LES implementations, it is unusual to adopt negative Boussinesq eddy viscosity to achieve SGS backscatter for stability considerations; therefore, a further issue that we address here is ability of SGS models to capture SGS backscatter.

2 Governing equations and computational setup

The simulations solve the continuity, momentum, and internal energy equations of ideal gas (with the equation of state being $p = \rho RT$, where $R = 8.31446$ [J/(mol · K)] is the universal gas constant),

$$\frac{\partial \rho}{\partial t} + \frac{\partial \rho u_j}{\partial x_j} = 0 \,, \tag{1}$$

$$\frac{\partial \rho u_i}{\partial t} + \frac{\partial \rho u_i u_j}{\partial x_j} = -\frac{\partial p}{\partial x_i} + \frac{\partial \sigma_{ij}}{\partial x_j} \,, \tag{2}$$

$$\frac{\partial \rho \varepsilon}{\partial t} + \frac{\partial \rho \varepsilon u_j}{\partial x_j} = -p\frac{\partial u_j}{\partial x_j} - \frac{\partial q_j^{\varepsilon}}{\partial x_j} + \sigma_{ij}\frac{\partial u_i}{\partial x_j} + \dot{\omega}_{\varepsilon} \,, \tag{3}$$

$$\frac{\partial \rho Y_i}{\partial t} + \frac{\partial \rho Y_i u_j}{\partial x_j} = -\frac{\partial q_j^{i}}{\partial x_j} + \dot{\omega}_i \,, \tag{4}$$

where $\sigma_{ij} = 2\mu\left(S_{ij} - \frac{1}{3}S_{kk}\delta_{ij}\right)$ is the shear stress of a Newtonian fluid, $S_{ij} = \frac{1}{2}\left(\frac{\partial u_i}{\partial x_j} + \frac{\partial u_j}{\partial x_i}\right)$ is the strain rate tensor, $q_j^{\varepsilon} = -\frac{\mu}{Pr}\frac{\partial \varepsilon}{\partial x_j}$ is the heat flux, Pr is the Prandtl number, $q_j^i = -\frac{\mu}{Sc_i}\frac{\partial Y_i}{\partial x_j}$ is the species flux, Sc_i is the Schmidt number for each species i, $\dot{\omega}_{\varepsilon}$ is the heat release in combustion reactions, and $\dot{\omega}_i$ is the mass reaction rate of the species. The reaction terms are simply omitted in non-reacting simulations.

The study focuses on a stoichiometric hydrogen-air mixture. We adopt the JANAF polynomial coefficients [14] to calculate the thermodynamic properties of the mixture. The viscosity is calculated based on the Sutherland's law, $\mu(T) = \mu_{ref}\left(\frac{T}{T_0}\right)^{3/2}\frac{T_0+S}{T+S}$, with $T_0 = 273.15$ [K], $S = 110.4$ [K] and μ_{ref} is set according to the Reynolds number. Considering the non-unity Lewis-number effects in hydrogen-air flames, we follow previous studies (e.g., [3]) and adopt a constant Prandtl number, $Pr = 0.7$, and four constant Schmidt numbers for four species: $Sc_{H_2} = 0.2$ ($Le_{H_2} = 0.29$), $Sc_{O_2} = 0.84$ ($Le_{O_2} = 1.2$), $Sc_{H_2O} = 0.66$ ($Le_{H_2O} = 0.94$), and $Sc_{N_2} = 0.75$ ($Le_{N_2} = 1.07$). These are approximate property values of air and species at 101325 [Pa] and 293.15 [K].

Although a detailed mechanism can deliver intermediate products in combustion, a one-step global reaction is often used in practical simulations to explore the basic behavior of combustion system due to its simplicity, and thus a simplified description of chemical kinetics is extremely useful for practical applications of combustion sciences to engineering problems [15]. Following previous study on the interaction between turbulence and reaction [1, 2], the study adopts a single-step irreversible Arrhenius mechanism [16, 1, 2] between fuel and oxidizer to provide realistic predictions of flame structure and heat release while requiring low computational cost, thereby allowing the high spatial resolution in DNS. The reaction formulation is $H_2 + 0.5O_2 \rightarrow H_2O$, and based on the global reaction model by Marinov et al. [16], the reaction rate expression is $K = A[H_2]^{1.0}[O_2]^{0.5}exp(-T_a/T)$, where $T_a = -17614$ [K], square brackets represent molar concentration, and the pre-exponential coefficient, A, is set according to the simulated combustion condition.

We solve the DNS equations (1, 2, 3, 4) by using the standard pseudo-spectral technique [17, 9, 18, 19] with the 2/3 de-aliasing rule [17] in a triply periodic cube with the resolution of N^3 Fourier modes. The time advance is carried out through the use of an explicit third-order Runge-Kutta scheme adopted in previous studies (e.g., [9, 19]). Note that, as the combustion progresses, the pressure inside the domain will increase as expected because of the heat release; however, the pressure gradient is the factor that actually affects momentum.

We employ a standard progress variable [13, 2] to initialize temperature and mass fractions of species, $c = (Y_{\mathrm{H}_2} - Y_{\mathrm{H}_2,u})/(Y_{\mathrm{H}_2,b} - Y_{\mathrm{H}_2,u}) = 1 - Y_{\mathrm{H}_2}/Y_{\mathrm{H}_2,u}$, where $Y_{\mathrm{H}_2,b} = 0$ and $Y_{\mathrm{H}_2,u} = 0.0284$ are the mass fractions of burnt and unburnt hydrogen. To set the initial temperature, we adopt the equation $T = c(T_b - T_u) + T_u$, where the unburnt temperature is $T_u = 300$ [K] and the burnt temperature is $T_b = 2200$ [K]. Likewise, for the initial mass fractions of oxygen and water vapor, we adopt the equations $Y_{\mathrm{O}_2} = (1-c)Y_{\mathrm{O}_2,u}$ and $Y_{\mathrm{H}_2\mathrm{O}} = cY_{\mathrm{H}_2\mathrm{O},b}$, where $Y_{\mathrm{O}_2,u} = 0.2264$ and $Y_{\mathrm{H}_2\mathrm{O},b} = 0.2548$ are the mass fractions of unburnt oxygen and burnt water-vapor.

We have carried out separate DNS of decaying compressible isotropic turbulence at a low Mach number ($Ma_t \sim 0.01$) to serve as the initial velocity conditions for the reacting cases. The composition of the non-reacting cases is the stoichiometric hydrogen-air mixture. Decaying compressible turbulent cases start with a synthetic state (e.g., [20]), and decay over

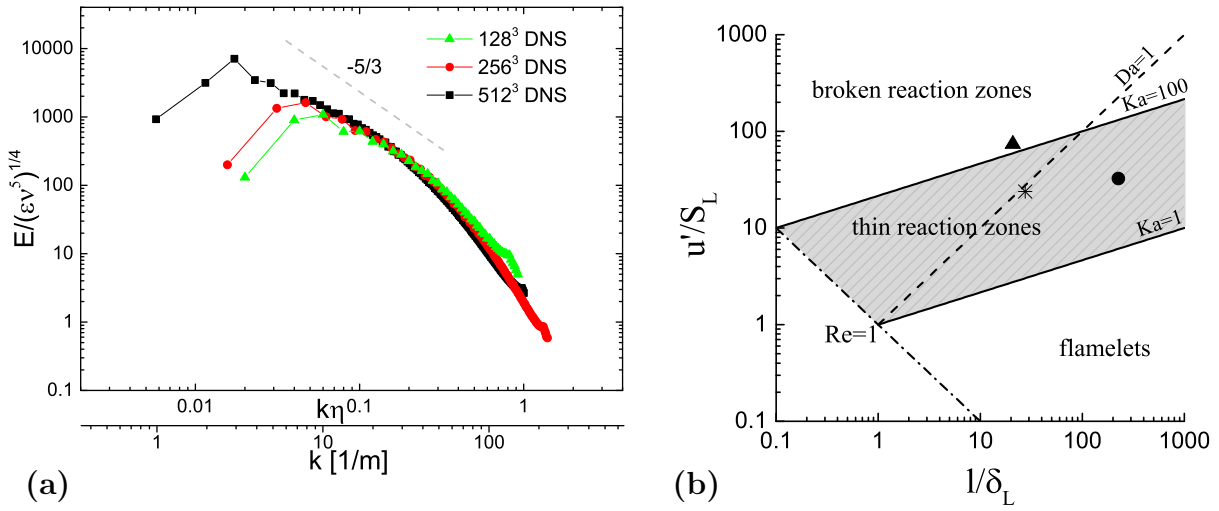

Figure 1: (a) Kinetic-energy spectra of three initial fields, and (b) combustion regime diagram [13] showing initial DNS locations: $*$: Case 1; ▲: Case 2; and •: Case 3.

more than five initial eddy-turn-over times. Figure 1(a) shows the normalized kinetic-energy spectra of three initial fields, and the agreement with the Kolmogorov -5/3 power-law scaling in the inertial subrange and the collapse in the dissipation range are reasonable.

3 Results

This section addresses the pressure effects on the interscale kinetic-energy transfer in premixed flames, and also presents *a priori* results of three SGS models for the SGS backscatter prediction. We consider two configurations: i) a spherical flame by considering a progress variable with a normal distribution at the center; and ii) kinetic-energy transfer from a particular scale by initializing a progress variable with a random field involving a Gaussian spectrum localized at a particular wavenumber, $\widehat{\mathcal{C}}(k) = \mathcal{E}\frac{\exp\left(-0.5(k-k_p)^2/\sigma^2\right)}{(2\pi)^{1/2}\sigma}$, where k_p is the peak wavenumber, σ is the standard deviation, and $\mathcal{E}$ is the magnitude rate. Following previous studies [9, 18, 19], we adopt $\sigma = 1$ and $\mathcal{E} = 1$. According to the Rankine-Hugoniot relation, there will be a certain pressure difference before and after the flame front, which is proportional to the square of the Mach number. For the purposes of this study, we focus on premixed flames with low Mach numbers; therefore, ignoring the initial pressure difference, we set the initial pressure as 101325 [Pa].

The corresponding laminar flame based on the same chemical mechanism and diffusion properties is characterized as the laminar flame speed S_l and the laminar flame width $\delta_l = (T_{l,b} - T_{l,u})/(dT/dx)_{max}$, where the burnt temperature, the unburnt temperature and the maximum temperature gradient are obtained in the corresponding laminar flame simulation. *These have been calculated by a separate in-house laminar flame code.* We compute the Damköhler and Karlovitz numbers as follows: $Da = \tau_e/\tau_c$ and $Ka = \tau_c/\tau_\eta$, where, $\tau_e = k/\varepsilon$ is the eddy-turn-over time, k is the turbulent kinetic energy (per unit mass), ε is the kinetic-energy dissipation rate (per unit mass), $\tau_\eta = (\nu/\varepsilon)^{1/2}$ is the Kolmogorov timescale, ν is the

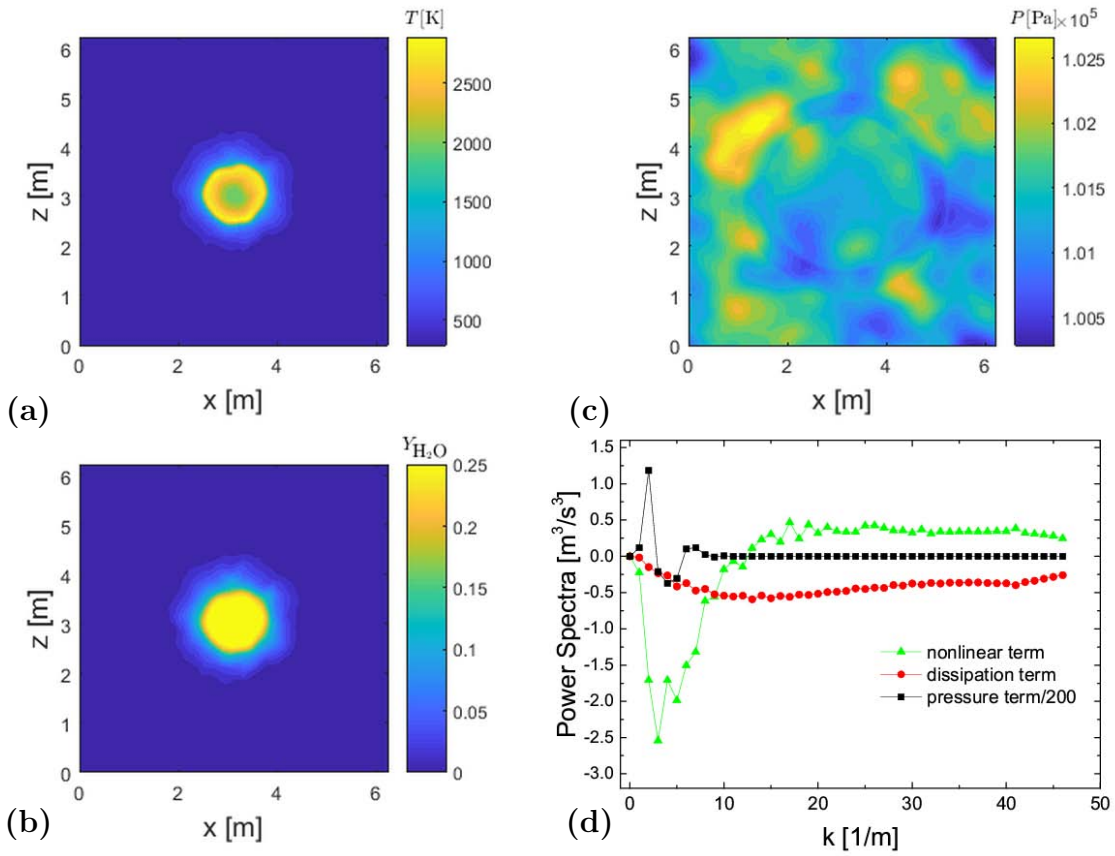

Figure 2: Contours of instantaneous (a) temperature, (b) mass fraction of water vapor, and (c) pressure, and (d) power spectra of $\widehat{\mathcal{N}}(k,t)$, $\widehat{\mathcal{P}}(k,t)$ and $\widehat{\varepsilon}(k,t)$ at t = 75 [ms] in Case 1.

averaged kinetic viscosity, and $\tau_c = \delta_l/S_l$ is the combustion time scale. Table 1 summarizes simulation-parameter values. Figure 1(b) shows the corresponding initial locations of the present DNSs on the combustion regime diagram, and figures 2(a-c) and 3 show the physical views of two simulated reacting flows, Case 1 and Case 3. It is important to note that all three cases fall into the region where the turbulence-combustion interactions are strong. Case 1 simulates the development of a single spherical flame in turbulence. Because the flame size is relatively large, the resolution of 128^3 is sufficient. Although the value of k_p is 20 [1/m] in both Case 2 and Case 3, the corresponding length scale of this wavenumber in Case 2 with the resolution of 256^3 is closer to the dissipation range, whereas in Case 3 with the resolution of 512^3, this wavenumber is in the inertial subrange. These conditions allow us to explore kinetic-energy transfer under the influence of different combustion scales relative to the turbulence scale. *The simulations have been performed on the Intel Xeon E5-2692 v2 supercomputers at the National Supercomputer Center in Guangzhou, and the 512^3 case requires 62 thousand CPU-hours running for approximately 10 days on 256 processors.*

Case	N^3	Re_λ	S_l [m/s]	δ_l [m]	Da	Ka	k_p [1/m]
1	128^3	80	0.3	0.126	1.15	22.3	(N.A.)
2	256^3	123	0.17	0.41	0.28	138.7	20
3	512^3	270	0.36	0.043	6.93	12.3	20

Table 1: Input model parameters including resolutions, initial Reynolds numbers based on the Taylor scale, initial values of Da and Ka, corresponding laminar flame speeds and widths, and peak wavenumber values for the progress-variable initialization.

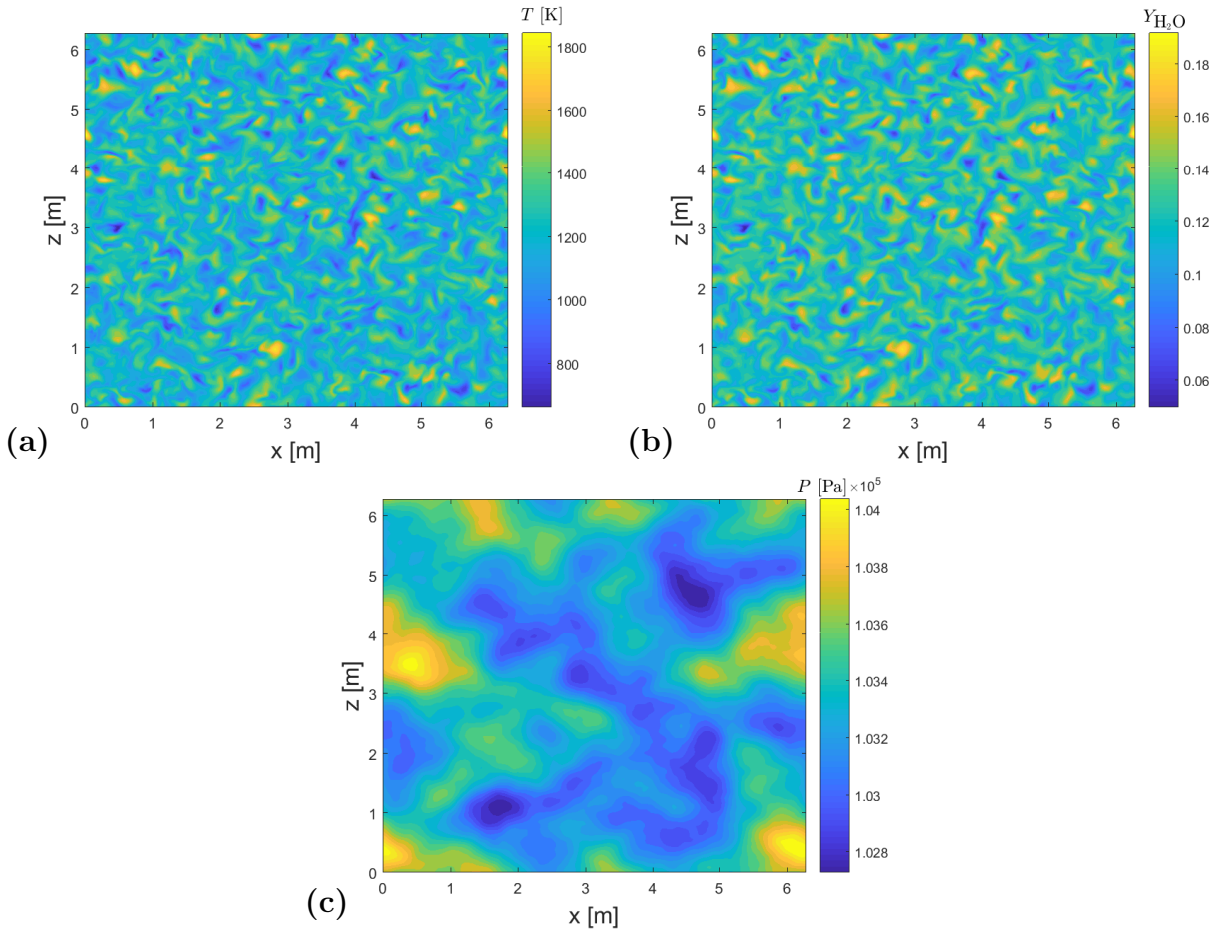

Figure 3: Instantaneous (a) temperature, (b) mass fraction of water vapor, and (c) pressure at t = 62.5 [ms] in Case 3.

3.1 Spectral kinetic energy dynamics

Here, we analyze the effects of premixed flames on interscale kinetic-energy transfer by using the kinetic-energy transport equation for reacting flow in Fourier space. First, we rewrite the momentum equation (2) as

$$\frac{\partial u_i}{\partial t} = \underbrace{-\,u_j \frac{\partial u_i}{\partial x_j}}_{\mathcal{N}_i} \underbrace{-\,\frac{1}{\rho}\frac{\partial p}{\partial x_i}}_{\mathcal{P}_i} \underbrace{+\,\frac{1}{\rho}\frac{\partial \sigma_{ij}}{\partial x_j}}_{\varepsilon_i}, \tag{5}$$

where $\mathcal{N}_i$ represents nonlinear advection processes, $\mathcal{P}_i$ represents pressure effects, and ε_i represents dissipations. When the variables on both sides of the equation are transformed into Fourier space, the spectral transport equation of velocities are: $\frac{\partial \widehat{u}_i(\mathbf{k},t)}{\partial t} = \widehat{\mathcal{N}}_i(\mathbf{k},t) + \widehat{\mathcal{P}}_i(\mathbf{k},t) + \widehat{\varepsilon}_i(\mathbf{k},t)$, where $\widehat{(\cdot)}$ denotes a 3D Fourier transform, and all of the terms in the above equation depend on the 3D wave-number vector $\mathbf{k} = (k_1, k_2, k_3)$ and time. The transport equation of turbulent kinetic energy in Fourier space is $\frac{\partial \widehat{E}(\mathbf{k},t)}{\partial t} = \frac{\partial \frac{1}{2}\widehat{u}_i^*(\mathbf{k},t)\widehat{u}_i(\mathbf{k},t)}{\partial t} = \frac{1}{2}\left(\widehat{u}_i^*(\mathbf{k},t)\frac{\partial \widehat{u}_i(\mathbf{k},t)}{\partial t} + \widehat{u}_i(\mathbf{k},t)\frac{\partial \widehat{u}_i^*(\mathbf{k},t)}{\partial t}\right)$, where $\widehat{u}_i^*$ is the complex conjugate of velocity. The transport equation of $\widehat{E}(\mathbf{k},t)$ can be derived as $\frac{\partial \widehat{E}(\mathbf{k},t)}{\partial t} = \widehat{\mathcal{N}}(\mathbf{k},t) + \widehat{\mathcal{P}}(\mathbf{k},t) + \widehat{\varepsilon}(\mathbf{k},t)$, where the terms on the right are given generically for a function $\widehat{\mathcal{F}}$ as $\widehat{\mathcal{F}} = \frac{1}{2}(\widehat{u}_i^*\widehat{\mathcal{F}_i} + \widehat{u}_i\widehat{\mathcal{F}_i^*})$. Statistics in isotropic turbulence are independent of direction, thus, we integrate in Fourier space over $k = |\mathbf{k}|$, and get

$$\frac{\partial \widehat{E}(k,t)}{\partial t} = \widehat{\mathcal{N}}(k,t) + \widehat{\mathcal{P}}(k,t) + \widehat{\varepsilon}(k,t)\ , \tag{6}$$

where $\widehat{\mathcal{N}}(k,t)$ is the nonlinear advection contribution, $\widehat{\mathcal{P}}(k,t)$ is the pressure transfer term, and $\widehat{\varepsilon}(k,t)$ is the dissipation term. In a non-reacting flow, the sum of $\widehat{\mathcal{N}}(k,t)$ and $\widehat{\mathcal{P}}(k,t)$ is often called the nonlinear energy-transfer function, $\widehat{\mathcal{T}}(k,t)$ [4]. This study distinguishes between the effects of nonlinear advection and the effects of pressure in particular, so we deliberately separate them. The dissipation term also includes the effects of density and viscous gradients caused by heat release in combustion reactions, but we do not extract them in this study.

Figure 2(c) shows an obvious expansion pressure wave caused by the central spherical flame. Pressure gradient is one main factor causing the change in velocity, so it is reasonable to believe that the pressure differences across the expansion wave will inevitably affect the kinetic energy. Figure 2(d) shows $\widehat{\mathcal{N}}(k,t)$, $\widehat{\mathcal{P}}(k,t)$ and $\widehat{\varepsilon}(k,t)$ appearing in Eqn. (6) at t = 75 [ms]. In the spectral analysis of these three budget terms, a positive value indicates a contribution to the increase in turbulent kinetic energy, while a negative value represents a contribution to the decrease in turbulent kinetic energy. It is clear that the magnitude of the pressure transfer term here at the largest scales, $k = 1 \sim 3$ [1/m] is significantly larger than the magnitude of the nonlinear advection (note that the pressure term in figure 2(d) is divided by a factor of 200). In line with previous findings on premixed flame [1], the energy transfer function, $\widehat{\mathcal{T}} = \widehat{\mathcal{N}} + \widehat{\mathcal{P}}$, bears positive values within the large-scale range, indicating energy transfers from smaller to larger scales. Moreover, current results reveal that in this case, the pressure transfer term yields the majority of contributions of the inverse kinetic-energy cascade.

Different from the reactions in Case 1, which contains a single spherical flame close to the integral length scale, reactions in Case 2 and Case 3 occur at smaller scales, specifically between the inertial scale and the dissipation scale (Case 2), and in the inertial scale (Case 3), respectively. Figures 4(a) and (c) show the power spectra of three terms obtained in two cases at one moment. Again, it is evident that the overall effect of the pressure-transfer term is to increase kinetic energy at large scales, and its magnitude is significantly larger than the magnitude of the nonlinear advection term. Furthermore, figures 4(b) and (d) show the time averaged power spectra of three terms. Results confirm that over a period of time, the pressure transfer term contributes kinetic energy at large scales. In contrast, the results

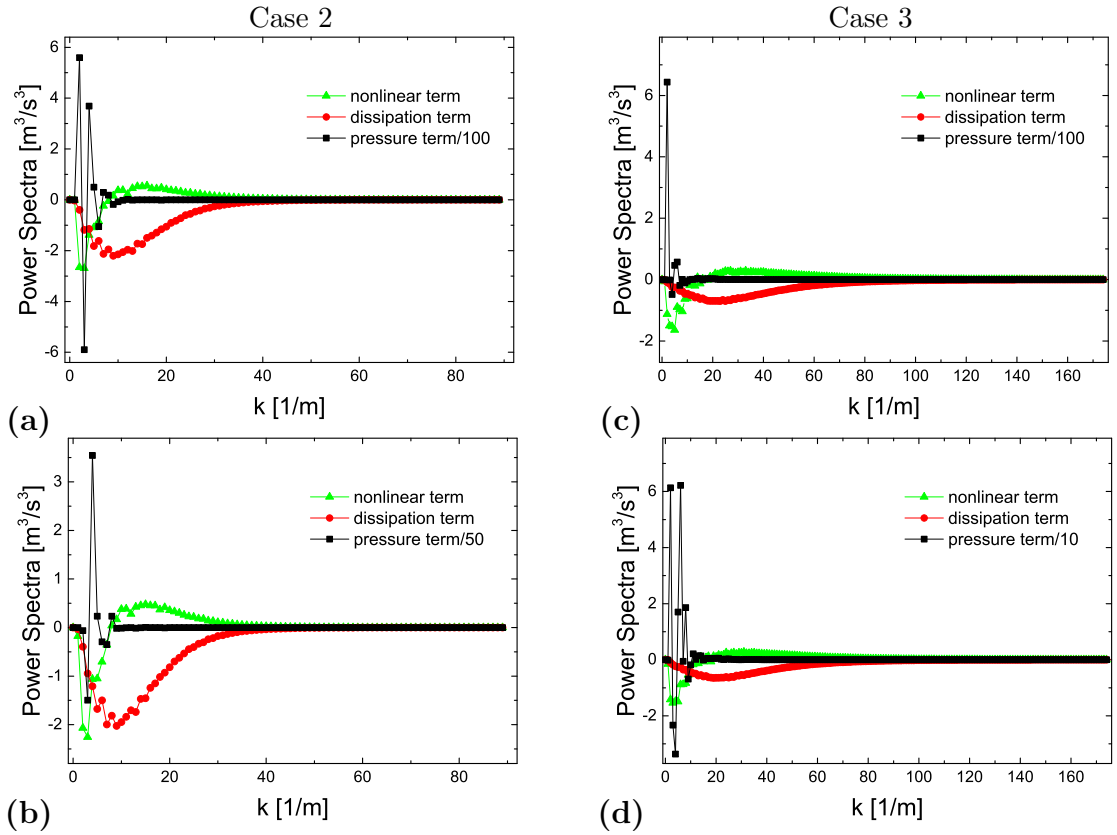

Figure 4: Power spectra of $\widehat{\mathcal{N}}(k,t)$, $\widehat{\mathcal{P}}(k,t)$ and $\widehat{\varepsilon}(k,t)$ (a) at t = 50 [ms] and (b) time averaged (over 30 [ms]) in Case 2, and (c) at t = 20 [ms] and (d) time averaged (over 21.2 [ms]) in Case 3.

show that the nonlinear term transfers energy from large to small scales, and the dissipation term dissipates all scales.

To better understand the interscale kinetic-energy transfer, we draw from Domaradzki and Carti [21] in calculating the energy flux of each term given generically for a function $\widehat{\mathcal{F}}$ as, $\Pi^{\widehat{\mathcal{F}}}(k,t) = \int_0^k \widehat{\mathcal{F}}(k',t)dk'$. The energy flux provides the energy-transfer rate from all scales below k to those above k, and a positive (negative) value of the energy flux represents that the wave-number shell at k is a net recipient (donor) of energy from all smaller scales. Figure 5 shows the time-averaged energy fluxes of three terms obtained in Case 2 and Case 3. In line with research on incompressible isotropic turbulence [4], our results show that the nonlinear advection does not produce or dissipate any kinetic energy in any of the scales, and it transfers energy only from large to small scales. The dissipation term dissipates kinetic energy over all scales. More importantly, it is evident that at the scales larger than $k = 10$ [1/m], the pressure transfer results in noticeable inverse transfers from all smaller scales.

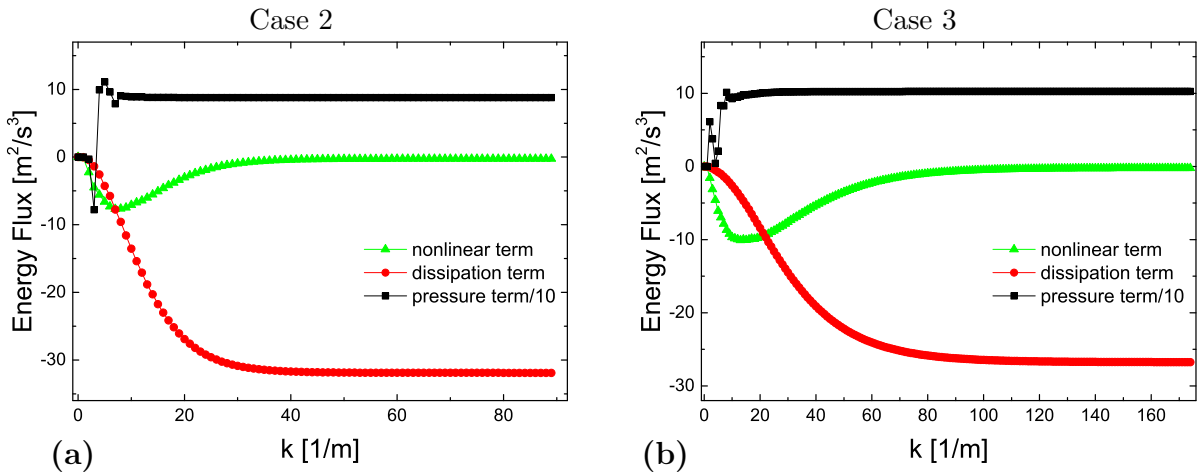

Figure 5: Time averaged energy flux spectra of $\widehat{\mathcal{N}}(k,t)$, $\widehat{\mathcal{P}}(k,t)$ and $\widehat{\varepsilon}(k,t)$ in Case 2 and Case 3.

3.2 SGS backscatter dynamics

The density-weighted (which defines the change of variables as: $\widetilde{f} = \frac{\overline{\rho f}}{\overline{\rho}}$) LES equations of momentum conservation are,

$$\frac{\partial \overline{\rho}\widetilde{u}_i}{\partial t} + \frac{\partial \overline{\rho}\widetilde{u}_i\widetilde{u}_j}{\partial x_j} = -\frac{\partial \overline{p}}{\partial x_i} - \frac{\partial \tau_{ij}}{\partial x_j} + \frac{\partial \overline{\sigma}_{ij}}{\partial x_j} \ , \tag{7}$$

where $\tau_{ij} = \overline{\rho}\left(\widetilde{u_i u_j} - \widetilde{u}_i\widetilde{u}_j\right)$ is the SGS stress tensor, which needs an SGS stress model to close. The SGS kinetic energy is $K_{sgs} = \frac{1}{2}\overline{\rho}\left(\widetilde{u_i u_i} - \widetilde{u}_i\widetilde{u}_i\right) = \frac{1}{2}\tau_{ii}$, and its transport equation [22] is,

$$\begin{aligned}\frac{\partial K_{sgs}}{\partial t} + \frac{\partial K_{sgs}\widetilde{u}_j}{\partial x_j} \ = \ & \underbrace{\left(\overline{p\frac{\partial u_j}{\partial x_j}} - \overline{p}\frac{\partial \widetilde{u}_j}{\partial x_j}\right)}_{\Pi_{sgs}} \underbrace{-\tau_{ij}\frac{\partial \widetilde{u}_i}{\partial x_j}}_{P_{sgs}} + \underbrace{\left(\overline{u_i\frac{\partial \sigma_{ij}}{\partial x_j}} - \widetilde{u}_i\frac{\partial \overline{\sigma_{ij}}}{\partial x_j}\right)}_{\varepsilon_{sgs}} \\ & \underbrace{-\frac{\partial}{\partial x_j}\left[\frac{1}{2}\overline{\rho}\left(\widetilde{u_i u_i u_j} - \widetilde{u}_i\widetilde{u}_i\widetilde{u}_j\right) - \tau_{ij}\widetilde{u}_i + \left(\overline{p u}_j - \overline{p}\widetilde{u}_j\right)\right]}_{D_{sgs}} \ ,\end{aligned} \tag{8}$$

where $\Pi_{sgs} = \left(\overline{p\frac{\partial u_j}{\partial x_j}} - \overline{p}\frac{\partial \widetilde{u}_j}{\partial x_j}\right)$ is the SGS pressure-dilatation term (often neglected in open-environment flames [23]), $P_{sgs} = -\tau_{ij}\frac{\partial \widetilde{u}_i}{\partial x_j} = -\tau_{ij}\widetilde{S}_{ij}$ is the SGS kinetic-energy production, $\varepsilon_{sgs} = \left(\overline{u_i\frac{\partial \sigma_{ij}}{\partial x_j}} - \widetilde{u}_i\frac{\partial \overline{\sigma_{ij}}}{\partial x_j}\right)$ is the SGS dissipation term (commonly modeled as $\varepsilon_{sgs} = -C_e\overline{\rho}\frac{k_{sgs}^{3/2}}{\Delta}$, where $k_{sgs} = K_{sgs}/\overline{\rho}$, $C_e = 1$ [19]), and the last term including the diffusion effects of the triple correlation, the SGS production, and the pressure-velocity correlation is often modeled as an SGS diffusion, $D_{sgs} = \frac{\partial}{\partial x_j}\left(\left(\mu_{sgs} + \mu\right)\frac{\partial k_{sgs}}{\partial x_j}\right)$, where $\mu_{sgs} = C_k\overline{\rho}\sqrt{k_{sgs}}\Delta$, $C_k = 0.05$ [19]. The SGS production term, P_{sgs}, represents the rate at which kinetic energy is transferred from resolved to subgrid scales. For the subgrid field, P_{sgs} is an energy production term,; but for the resolved field, it is a dissipation term of kinetic energy and is therefore also known as

the SGS dissipative term [3]. The SGS production can be locally negative, $P_{sgs} < 0$, which corresponds to the inverse transfer of kinetic energy from subgrid to resolved scale (i.e., SGS backscatter) [10, 6]. We define the backscatter SGS production as $P_{sgs,b} = H(-P_{sgs})\,P_{sgs}$, where $H(x)$ is the Heaviside step function. Moreover, previous studies [3, 2] have shown that SGS backscatter occurs primarily in regions undergoing volumetric expansion. In this study, we investigate the relationship between the backscatter SGS production and the resolved pressure-dilatation work, which is defined as $\Pi = \overline{p}\frac{\partial \widetilde{u}_i}{\partial x_i}$. Depending on the sign of the flow dilatation, the positive (negative) Π represents expansion (compression).

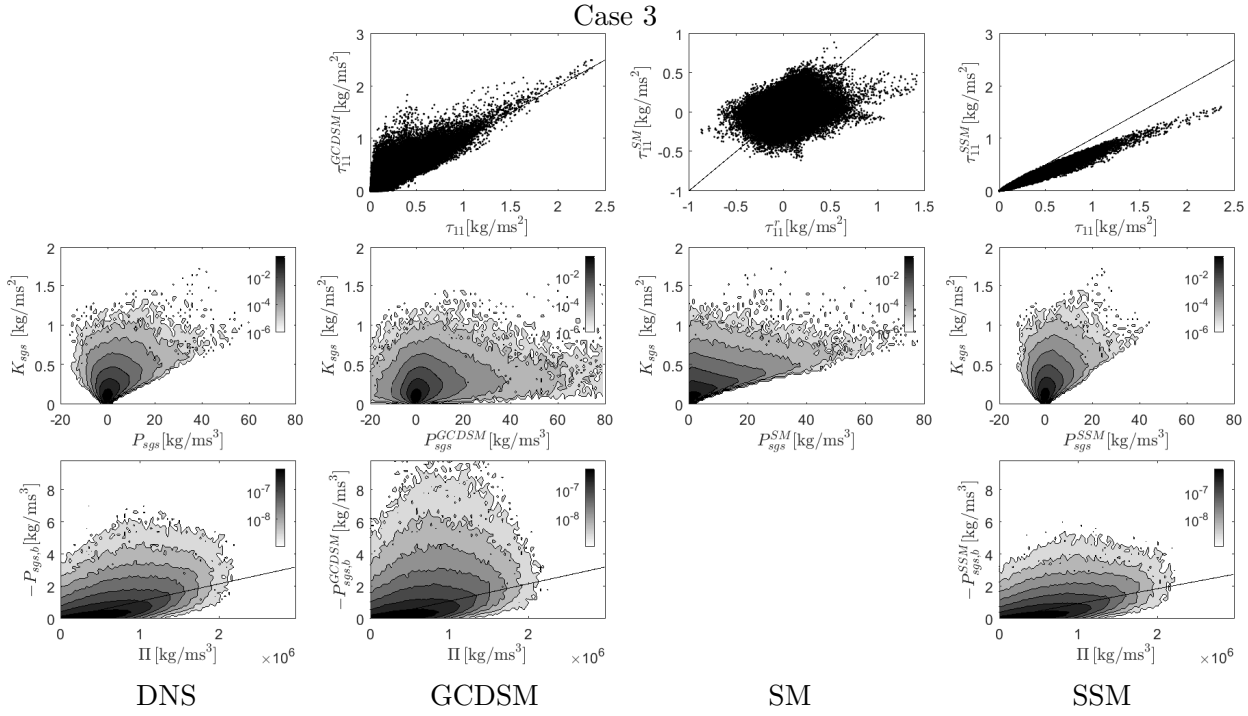

Figure 6: *A priori* results in Case 3: (first row) scatter plots of exact and modeled SGS stresses, (second row) joint PDFs between SGS kinetic energy and SGS production, and (third row) joint PDFs between backscatter SGS production and resolved pressure-dilatation work. Note that the first column shows results from the filtered DNS data, the second column shows the predictions using the GCDSM, the third column shows the predictions using the SM (no backscatter SGS productions are available using the SM), and the last column shows the predictions using the SSM.

Figures 6 and 7 show *a priori* test results obtained by filtering the DNS data using the Gaussian filter with the width, $\Delta = \pi/k_c$, corresponding to a wavenumber of $k_c = 40$ [1/m] in Case 3 and Case 2. The joint probability density function (PDF) between K_{sgs} and P_{sgs} bears a structure similar to that noted in previous studies [2, 24], and the negative region of P_{sgs} is observable, indicating the existence of SGS backscatter. Moreover, in line with O'Brien et al. [3], there exists noticeable correlation (the value of the correlation coefficient is 0.51) between $P_{sgs,b}$ and positive Π, indicating that the backscatter SGS production region is correlated with the thermal expansion in Case 3. But the correlation between $P_{sgs,b}$ and positive Π is 0.4 in Case 2. One possible reason is that case 2 bears stronger turbulence-combustion interactions since its Ka is higher. Further studies are needed to reveal the

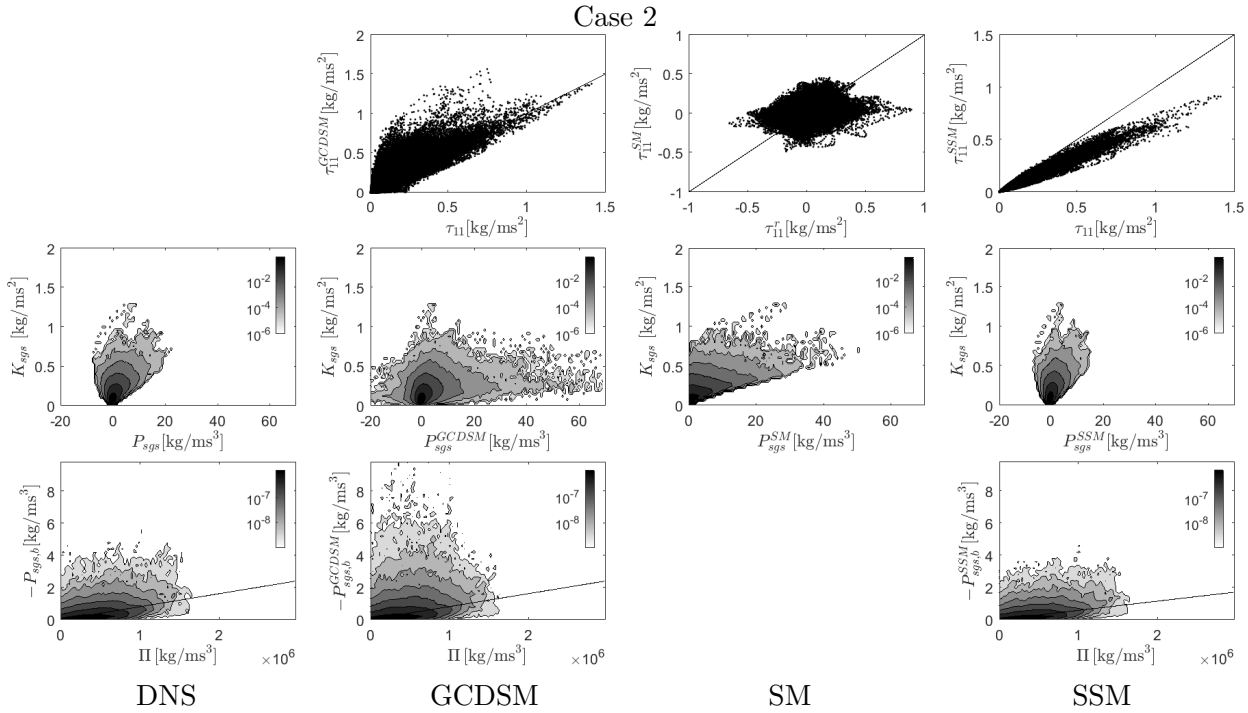

Figure 7: *A priori* results in Case 2. Refer to the caption in figure 6 for details.

specific reasons for this difference.

In comparing the ability of typical SGS stress models to capture backscatter, we investigate three SGS stress models at the *a priori* test level. Based on the Boussinesq hypothesis, the first introduced SGS stress model, the Smagorinsky model (SM) [25] parameterizes the SGS stress' deviatoric (residual) part [12] as $\tau_{ij}^r = \tau_{ij} - \frac{1}{3}\delta_{ij}\tau_{kk} = -2\overline{\rho}\nu_{sgs}\widetilde{S}_{ij}$, where $\nu_{sgs} = C_s^2\Delta^2|\widetilde{S}|$ is the SGS eddy viscosity, $|\widetilde{S}| = (2\widetilde{S}_{ij}\widetilde{S}_{ij})^{1/2}$ is the strain rate, and the Smagorinsky coefficient, C_s, is a dimensionless coefficient in a range of 0.1 to 0.2 [12]. Here, we adopt $C_s = 0.17$. It is necessary to note that the value of the coefficient affects not the correlation calculation, but only the magnitude of the modeled SGS stress. Two nonlinear structural SGS stress models [6] are examined here. To resolve the issue of low correlation [18] between the exact and modeled SGS stress terms, researchers since 1980 [26, 12] have used the scale similarity model (SSM), $\tau_{ij} = \overline{\rho}\left(\widetilde{\widetilde{u}_i\widetilde{u}_j} - \widetilde{\widetilde{u}}_i\widetilde{\widetilde{u}}_j\right)$. It has been found at the tensor level, the modeled SGS stress tensor by using the SM or the SSM is not material-frame-indifference consistent with the exact SGS stress tensor [18, 19]. To resolve this lack of consistence, researchers since 2007 [18, 19] have introduced the gradient-type consistent dynamic structure model (GCDSM), $\tau_{ij} = 2K_{sgs}\left(\frac{\widetilde{G}_{ij}}{\widetilde{G}_{mm}}\right)$, where $\widetilde{G}_{ij} = \frac{\widetilde{\Delta}^2}{12}\frac{\partial\widetilde{u}_i}{\partial x_m}\frac{\partial\widetilde{u}_j}{\partial x_m}$ is the leading terms of the Taylor expansions of the exact SGS stress.

The second, third and fourth columns of figures 6 and 7 show - by means of the GCDSM, the SM and the SSM, respectively - 1) the scatter plots of the exact and predicted SGS stress τ_{11} components, 2) joint PDFs between the SGS kinetic energy and the predicted SGS production, and 3) joint PDFs between the predicted backscatter SGS productions and the positive resolved pressure-dilatation work in Cases 2 and Case 3. In line with previous *a priori* studies [18], the GCDSM and the SSM can yield quite satisfactory predictions on the

SGS stresses, whereas the SM fails in this regard. Specifically, the correlation coefficients between the exact and predicted SGS stress τ_{11} components using the GCDSM, the SSM and the SM (for the residual part) are 0.90, 0.98 and 0.24 in Case 3 and 0.88, 0.97 and 0.26 in Case 2. More importantly, the SM cannot yield negative P_{sgs}; in other words, the SM cannot predict SGS backscatter. In contrast, as two representatives of the structural SGS model, both the GCDSM and the SSM both can predict SGS backscatter. The reason for this difference is that the SGS eddy-viscosity approach rests the assumption that the energy-transfer mechanism is analogous to the molecular mechanism represented by dissipation in the momentum equations and by diffusion in scalar equations; therefore, the eddy-viscosity stress model, like the dissipation term shown in figures 4 and 5, can allow the kinetic-energy transfer only from large to small scales.

To the first-row plots in figures 6 and 7, we have added the expected regression lines (with a slope value of 1 indicating that the modeled term is identical to the exact term), and to the third-row plots in these figures, we have added the regression lines. The two examined structural SGS models have different issues: the GCDSM results in over-predictions of P_{sgs} at low turbulent levels; and the SSM results in underestimations of the SGS stress, leading to underestimations of SGS backscatter. Moreover, the implementation of the SSM requires a test filtering, which is computationally expensive. By contrast, the implementation of the GCDSM requires only velocity gradients, making the cost of the GCDSM similar to that of the SM. The modifications of the GCDSM have been applied to LESs involving a variety of turbulence types [19, 27, 22, 24, 28]. Results show that these applications can ensure not only low grid sensitivity, but high accuracy as well. Through these *a posteriori* practices, it is further shown that the prediction of inverse energy cascade (see the Appendix) is important to accurately simulation turbulent combustion, especially under high Reynolds number conditions.

4 Conclusions

Based on well-resolved DNS data of premixed isotropic flames, the results presented herein show that there exists inverse kinetic-energy transfer from small to large scales in flames, and that the pressure-transfer term is an important contributor in the transfer. Our *a priori* analyses of the joint PDFs between backscatter SGS production and pressure-dilatation work show that, in premixed isotropic flames, SGS backscatter also occurs primarily in regions undergoing expansion. *A priori* test results of three representative SGS stress models show that although the eddy-viscosity approach cannot yield SGS backscatter, two examined nonlinear structural models are evidently able to capture this mechanism. This outcome implies to some extent that in the LES of high-Reynolds-number turbulent combustion, the nonlinear SGS approach could be more reliable than the eddy-viscous SGS approach.

Further studies would do well to focus on the effects of Mach, Lewis, and Karlovitz numbers on energy transfer, and the effects of density and viscosity fluctuations caused by heat release in reactions on energy transfer.

Acknowledgments

This research was supported by the National Natural Science Foundation of China (51776082). Computing resources were provided by the National Supercomputer Center in Guangzhou.

Appendix: *a posteriori* results of Sandia Flame F simulations

It is important to test how well SGS stress models accurately reproduce turbulence characteristics of flows. In this way, one can understand whether or not a corresponding LES can capture stochastic processes and flow dynamics. For the purpose of comparison, we assess results obtained using the SM [25], and the mixed-version of the GCDSM [19] in simulating Sandia Flame F. Note that the mixed hyper-viscosity term is significantly smaller than the structural term [18, 19], and only plays the role of making the simulated flow stable at small scales. The details of the case and simulation results have been reported previously [22], and here we present the models' characteristics regarding the prediction of backscatter. Figure 8 compares the SM results with the results using the mixed-version of the GCDSM in predicting instantaneous SGS kinetic energy production. To demonstrate the difference between the structural stress model and the eddy-viscosity stress model, we set two contour plots in a range extending approximately from -40000 to 800000 [kg/ms^3]. The SM cannot yield negative P_{sgs}. This fact implies that the SM always delivers energy from resolved to subgrid scales. Thus, the mechanism for the mixing of small eddies into large eddies must be undertaken by the resolved field. This mixing would be a significant issue for simulating high-Reynolds-number flows, and would certainly reduce the accuracy in efforts to capture large-scale flows. Different from the eddy-viscosity/diffusivity approach, the nonlinear SGS approach consists mainly of two parts, a model for the magnitude of the corresponding SGS term, and a normalized gradient term to determine its structure, i.e., the relative magnitude of the different components. As expected, the adopted structural SGS stress model can provide negative SGS productions, which represent reverse energy transfers from subgrid to resolved scales, and are particularly important for the formation of large-scale coherent structures, such as Kelvin-Helmholtz vortices, in turbulent mixing layers. Further, the mixed-version of the GCDSM solves the transportation of k_{sgs}, and thus we can show the joint characteristics of k_{sgs} and P_{sgs}. As shown in figure 9(b), the SGS backscatter region, $P_{sgs} < 0$, is clearly evident. Figure 9(a) shows the magnitude of mean backscatter SGS production predicted using the NLES. This magnitude exhibits a significant peak between $x/D = 10$ and $x/D = 20$. Previous studies (e.g. [22]) have shown that this height range is also the region where the extinction and re-ignition phenomenon is most intense.

References

[1] C. Towery, A. Poludnenko, J. Urzay, J. O'Brien, M. Ihme, and P. Hamlington, "Spectral kinetic energy transfer in turbulent premixed reacting flows," *Phys. Rev. E*, vol. 93, p. 053115, 2016.

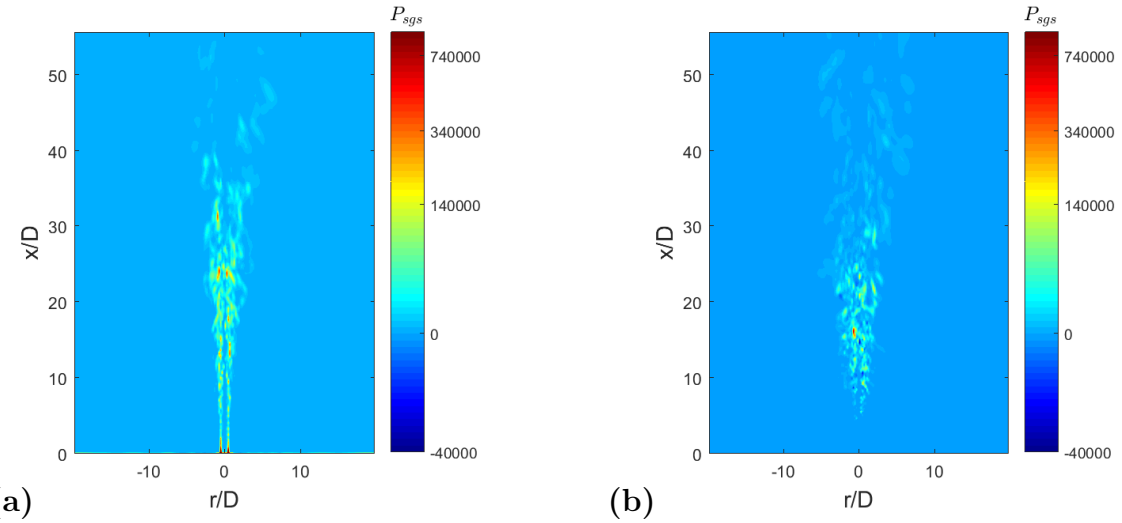

Figure 8: Filled contours of instantaneous SGS production computed using (a) the SM and (b) the NLES.

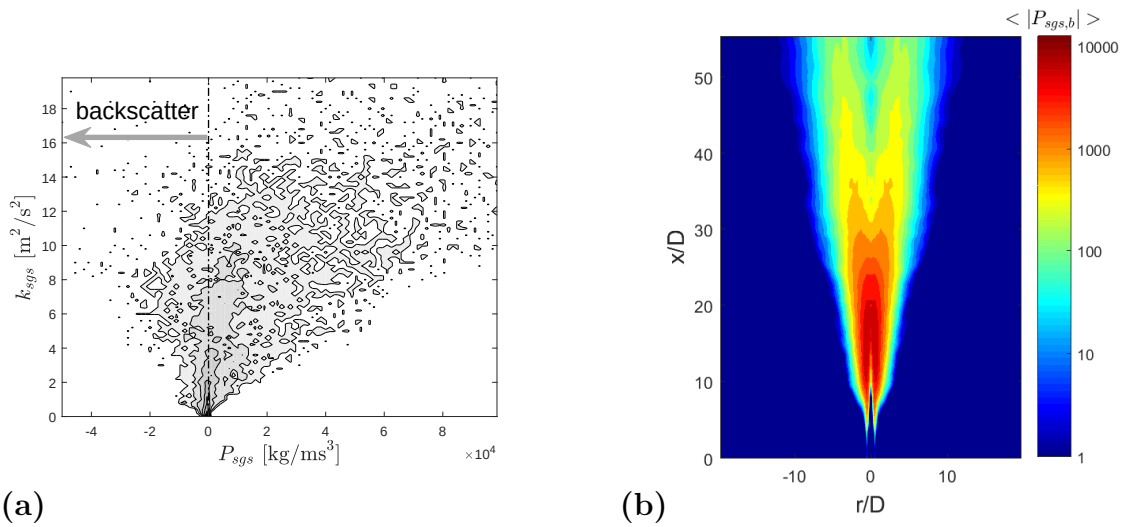

Figure 9: (a) Joint PDF of P_{sgs} and $k_{sgs} = K_{sgs}/\overline{\rho}$ obtained using the NLES at the height of $x/D = 15$; (b) filled contours of mean backscatter SGS production obtained using the NLES.

[2] J. O'Brien, C. A. Towery, P. E. Hamlington, M. Ihme, A. Y. Poludnenko, and J. Urzay, "The cross-scale physical-space transfer of kinetic energy in turbulent premixed flames," *Proc. Combust. Inst.*, pp. 1967–1975, 2017.

[3] J. O'Brien, J. Urzay, M. Ihme, P. Moin, and A. Saghafian, "Subgrid-scale backscatter in reacting and inert supersonic hydrogen-air turbulent mixing layers," *J. Fluid Mech.*, vol. 743, pp. 554–584, 2014.

[4] J. G. Brasseur and C.-H. Wie, "Interscale dynamics and local isotropy in high reynolds

number turbulence within triadic interactions," *Phys. Fluids*, vol. 6, p. 842, 1994.

[5] J. A. Domaradzki and E. M. Saiki, "Backscatter models for large-eddy simulations," *Theoret. Comput. Fluid Dynamics*, vol. 9, pp. 75–83, 1997.

[6] H. Lu and C. J. Rutland, "Structural subgrid-scale modeling for large-eddy simulation: A review," *Acta Mech. Sin.*, vol. 32, no. 4, pp. 567–578, 2016.

[7] J. Furukawa, K. Okamoto, and T. Hirano, "Turbulence characteristics within the local reaction zone of a high-intensity turbulent premixed flame," *26th Symp. (Int.) Comb.*, pp. 405–412, 1996.

[8] H. Kolla, E. R. Hawkes, A. R. Kerstein, N. Swaminathan, and J. H. Chen, "On velocity and reactive scalar spectra in turbulent premixed flames," *J. Fluid Mech.*, vol. 754, p. 456, 2014.

[9] L. M. Smith and F. Waleffe, "Generation of slow large scales in forced rotating stratified turbulence," *J. Fluid Mech.*, vol. 451, pp. 145–168, 2002.

[10] U. Piomelli, W. H. Cabot, P. Moin, and S. Lee, "Subgrid-scale backscatter in turbulent and transitional flows," *Phys. Fluids A*, vol. 3, pp. 1766–1771, July 1991.

[11] B. Vreman, B. Geurts, and H. Kuerten, "Large-eddy simulation of the turbulent mixing layer," *J. Fluid Mech.*, vol. 339, pp. 357–390, 1997.

[12] S. B. Pope, *Turbulent flows*. Cambridge University Press, Cambridge, 2000.

[13] N. Peters, *Turbulent combustion*. Cambridge University Press, Cambridge, 2002.

[14] R. Kee, F. Ripley, and J. Miller, "The CHEMKIN thermodynamic database," *Sandia Report SAND87-8215*, 1987.

[15] S. McAllister, J. Chen, and A. Fernandez-Pello, *Fundamentals of Combustion Processes*. Springer, New York, 2011.

[16] N. M. Marinov, C. K. Westbrook, and W. J. Pitz, "Detailed and global chemical kinetics model for hydrogen," *Office of Scientific and Technical Information Technical Reports*, 1995.

[17] C. Canuto, M. Y. Hussaini, A. Quarteroni, and T. A. Zang, *Spectral methods in fluid dynamics*. Springer-Verlag, Berlin Heidelberg, 1988.

[18] H. Lu, C. J. Rutland, and L. M. Smith, "A priori tests of one-equation LES modeling of rotating turbulence," *J. Turbul.*, vol. 8, no. 37, pp. 1–27, 2007.

[19] H. Lu, C. J. Rutland, and L. M. Smith, "A posteriori tests of one-equation LES modeling of rotating turbulence," *Int. J. Mod. Phys. C*, vol. 19, pp. 1949–1964, 2008.

[20] R. Samtaney, D. I. Pullin, and B. Kosović, "Direct numerical simulation of decaying compressible turbulence and shocklet statistics," *Phys. Fluids*, vol. 13, no. 5, pp. 1415–1430, 2001.

[21] J. A. Domaradzki and D. Carati, "An analysis of the energy transfer and the locality of nonlinear interactions in turbulence," *Phys. Fluids*, vol. 19, p. 085112, 2007.

[22] H. Lu, W. Chen, C. Zou, and H. Yao, "Large-eddy simulation of Sandia Flame F using structural subgrid-scale models and partially-stirred-reactor approach," *Phys. Fluids*, vol. 31, p. 045109, 2019.

[23] E. Garnier, N. Adams, and P. Sagaut, *Large eddy simulation for compressible flows*. Springer Netherlands, 2009.

[24] S. Shao, H. Lu, Z. Wang, and X. Cheng, "Large-eddy simulation of high-speed vaporizing liquid-fuel spray using mixed gradient-type structural subgrid-scale model," *Combustion Science and Technology*, vol. 193, no. 5, 2021.

[25] J. Smagorinsky, "General circulation experiments with the primitive equations: I. the basic experiment," *Mon. Weather Rev.*, vol. 91, no. 3, pp. 99–164, 1963.

[26] J. Bardina, J. H. Ferziger, and W. C. Reynolds, "Improved subgrid scale models for large eddy simulation," *AIAA Paper No. 80-1357*, 1980.

[27] H. Lu, C. Zou, S. Shao, and H. Yao, "Large-eddy simulation of MILD combustion using partially stirred reactor approach," *Proc. Combust. Inst.*, vol. 37, no. 4, pp. 4507–4518, 2019.

[28] X. Qian, H. Lu, C. Zou, H. Zhang, S. Shao, and H. Yao, "A numerical investigation of the effects of turbulence on the ignition process in a turbulent MILD flame," *Acta Mech. Sin. (accepted)*, 2021.